PERGAMON

Journal of Structural Geology 22 (2000) 713–722

JOURNAL OF STRUCTURAL GEOLOGY

www.elsevier.nl/locate/jstrugeo

Geometrical classification of conjugate vein arrays

Deepak C. Srivastava

Department of Earth Sciences, University of Roorkee, Roorkee 247667, India

Received 29 July 1999; accepted 21 January 2000

Abstract

A classification of conjugate vein arrays is proposed on the basis of three angular parameters that can be readily measured at outcrops. Relationships amongst these parameters imply that geometry of conjugate vein arrays varies within a continuous spectrum limited by three end-members.

A new triangular plot is devised for representation of conjugate vein arrays, and its application is substantiated by several published and new examples. Evidence from overprinting relationships and consistency in the orientations of principal stresses imply that different types of conjugate vein arrays can develop in a common stress system.

1. Introduction

Deformation in layered sedimentary sequences is commonly accommodated in discrete structural zones exemplified by conjugate pairs of en-échelon vein arrays (Ramsay and Graham, 1970; Weiss, 1972; Rixon et al., 1983; Collins and De Paor, 1986; Dietrich, 1989; Price and Cosgrove, 1990; Sibson, 1996; Smith, 1996, 1997; Kelly et al., 1998 and others). A proper understanding of the geometrical variations in such conjugate vein arrays is fundamental for arriving at their dynamic interpretation (Roering, 1968; Beach, 1975; Rickard and Rixon, 1983; Rothery, 1988; Smith, 1996). In this article, I use the geometrical relationships and graphical displays of the angular variables to demonstrate that the geometry of conjugate vein arrays varies within a continuous spectrum. The validity of the newly devised triangular plot is attested by several published, and new examples from the Chittaurgarh area in Rajasthan, India and the Mumbles area in the eastern Gower Peninsula, UK.

2. Classification of conjugate vein arrays

Beach (1975) classified conjugate pairs of vein arrays into two geometrical types: (i) type-1 pairs in which veins in each array are parallel to the boundary (enveloping surface of veins) of the complementary array (Fig. 1a), and (ii) type-2 pairs in which veins in both the arrays are parallel to each other, irrespective of the orientation of the array boundaries (Fig. 1b).

According to Smith (1996), a conjugate pair is designated as convergent, or, divergent, depending upon whether the geometrical arrangement of the veins conforms to the pattern of a convergent or divergent fan, respectively (Fig. 1d and e). The degree of convergence or divergence in a conjugate pair is controlled by the relationship between the array dihedral angle θ and vein-array angle δ (Fig. 1a). Consideration of the θ–δ relationships leads to a five-fold classification of conjugate vein arrays (fig. 2 in Smith, 1996); namely, (i) divergent pairs ($\theta > 2\delta$), (ii) bisector-parallel pairs ($\theta = 2\delta$), (iii) weakly convergent pairs ($2\delta > \theta > \delta$), (iv) cross-parallel pairs ($\theta = \delta$), and (v) strongly convergent pairs ($\theta < \delta$). Cross-parallel pairs and bisector-parallel pairs in Smith's classification correspond to type-1 pairs and type-2 pairs in Beach's classification (Table 1).

E-mail address: dpkes@rurkiu.ernet.in (D.C. Srivastava).

0191-8141/00/$ - see front matter
PII: S0191-8141(00)00005-5

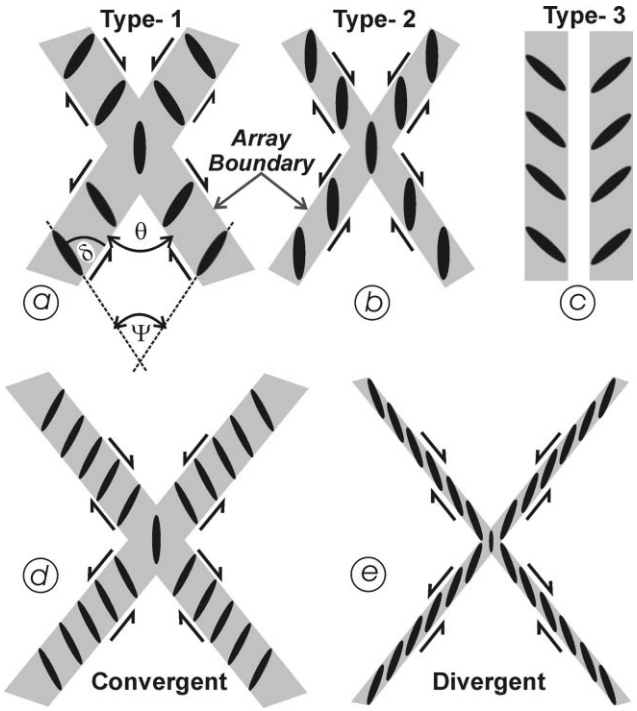

Fig. 1. Schematic diagrams for nomenclature of conjugate vein arrays. (a) and (b) Type-1 and type-2 pairs (after Beach, 1975). Three angular parameters; namely, array dihedral angle θ, vein-array angle δ and inter-vein angle ψ are defined in (a). (c) Type-3 conjugate pair. (d) and (e) Convergent and divergent configurations of conjugate arrays (after Smith, 1996).

3. Proposed classification

Three angular parameters can be measured readily on the profile section, i.e. the plane normal to the line of intersection of two array boundaries of a conjugate pair. These are: (i) the array dihedral angle θ, (ii) vein-array angle δ, and (iii) the inter-vein angle ψ, the latter being the angle between veins in the two arrays (Fig. 1a). Each set of the three angular parameters defines the complete geometry of a conjugate pair. Numerous patterns of conjugate arrays that are possible for different values of θ, δ and ψ, constitute a continuous geometric spectrum, which is limited by three end-members; namely, type-1, type-2 (vein-parallel), and type-3 (zone-parallel), pairs (Fig. 1a–c). The geometries of type-1, type-2 and type-3 pairs are constrained by the conditions $\theta = \delta = \psi$, $\psi = 0^\circ$ and $\theta = 2\delta$, and $\theta = 0^\circ$ and $\psi = 2\delta$, respectively.

Type-3 arrangement is, however, only a geometrical end-member in this classification. Development of such an arrangement is not mechanically possible, as it requires opposite sense of shearing on two arrays that are conjugate and yet parallel to each other. Although some conjugate pairs that are characterised by low array dihedral angle ($\theta \leq 20^\circ$) tend to approach a type-3 arrangement they can never, in strict sense, achieve it. A correlation between different nomenclatures of conjugate vein arrays and their relative abundance in natural rocks is summarised in Table 1.

4. Triangular plot

Three angular parameters in any convergent pair of conjugate vein arrays are related by the following equation:

$$\theta - 2\delta + \psi = 0. \quad (1)$$

Eq. (1) can be rearranged in following forms:

$$\theta/2 - \delta + \psi/2 = 0 \quad (2)$$

or

$$\theta/2 + (90 - \delta) + \psi/2 = 90. \quad (3)$$

Eq. (3) implies that any convergent pair of vein arrays can be plotted as a point on an equilateral triangle (Fig. 2a). The angles $\theta/2$, $(90 - \delta)$ and $\psi/2$ are equal to 90° at the three vertices of the triangle and they decrease progressively down to 0° along the normals dropped from their respective vertices, N, O and M, onto the opposite sides, MO, MN and NO (Fig. 2b–d).

Observations on natural examples reveal that three geometric conditions are always satisfied in a conjugate vein array: (i) the dihedral angle between the two array boundaries on which direction of movement is towards their intersection is always acute, i.e. $\theta \leq 90^\circ$, (ii) the inter-vein angle facing the acute dihedral angle

Table 1
Nomenclature of conjugate vein arrays and their relative abundance

Beach (1975)	Smith (1996)	This article	Occurrence in natural rocks
Type-1	Cross-parallel	Type-1(Cross-parallel)	Abundant
Type-2	Bisector-parallel	Type-2(Vein-parallel)	Occasional
–	–	Type-3(Zone-parallel)	Absent
–	Weakly convergent	Type 1 → 2(Transitional)	Common
–	–	Type 1 → 3(Transitional)	Common
–	Strongly convergent	Strongly convergent	Rare to absent
–	Divergent	Divergent	Absent

is also always acute, i.e. $\psi \leq 90^\circ$, and (iii) a divergent configuration of conjugate vein arrays has not yet been reported. Conditions (i) and (ii) justify the criterion that only acute dihedral- and inter-vein angles are taken into account for representation of conjugate arrays on the triangular graph. As a consequence, no conjugate pair ever plots within the regions NCD and MBD of the triangular graph (Fig. 2a, b and d). Furthermore, all the realistic types of conjugate vein arrays must plot only within a small rhombus-shaped region, OBDC in Fig. 2(a). As type-1, type-2 and type-3 pairs are characterised by the conditions, $\theta = \delta = \psi$, $\psi = 0^\circ$ and $\theta = 0^\circ$, respectively, their plots fall on the longer diagonal OD, and the sides OC and OB of the rhombus OBCD (Fig. 2a). Conjugate vein arrays with geometries that are transitional between type-1 and type-2 pairs (type-1 → 2), and type-1 and type-3 pairs (type-1 → 3) plot within the sub-triangles OCD and OBD, respectively (Fig. 2a).

For divergent pairs of conjugate vein arrays, the three angular parameters are related by the following equation:

$$\psi + 2\delta - \theta = 0 \tag{4}$$

or

$$\psi/2 + \delta + (90 - \theta) = 90. \tag{5}$$

Eq. (5) implies that divergent pairs can also be plotted on an equilateral triangular graph, such that, the $\psi/2$, δ and $(90-\theta)$ angles are equal to 90° at the three vertices of the triangle. As divergent configurations of conjugate vein arrays have not been reported and their mechanical viability is doubtful, the practical significance of this plot is limited. Angular variables in type-2 pairs of conjugate vein arrays satisfy both Eqs. (3) and (5) because such pairs delimit the geometrical

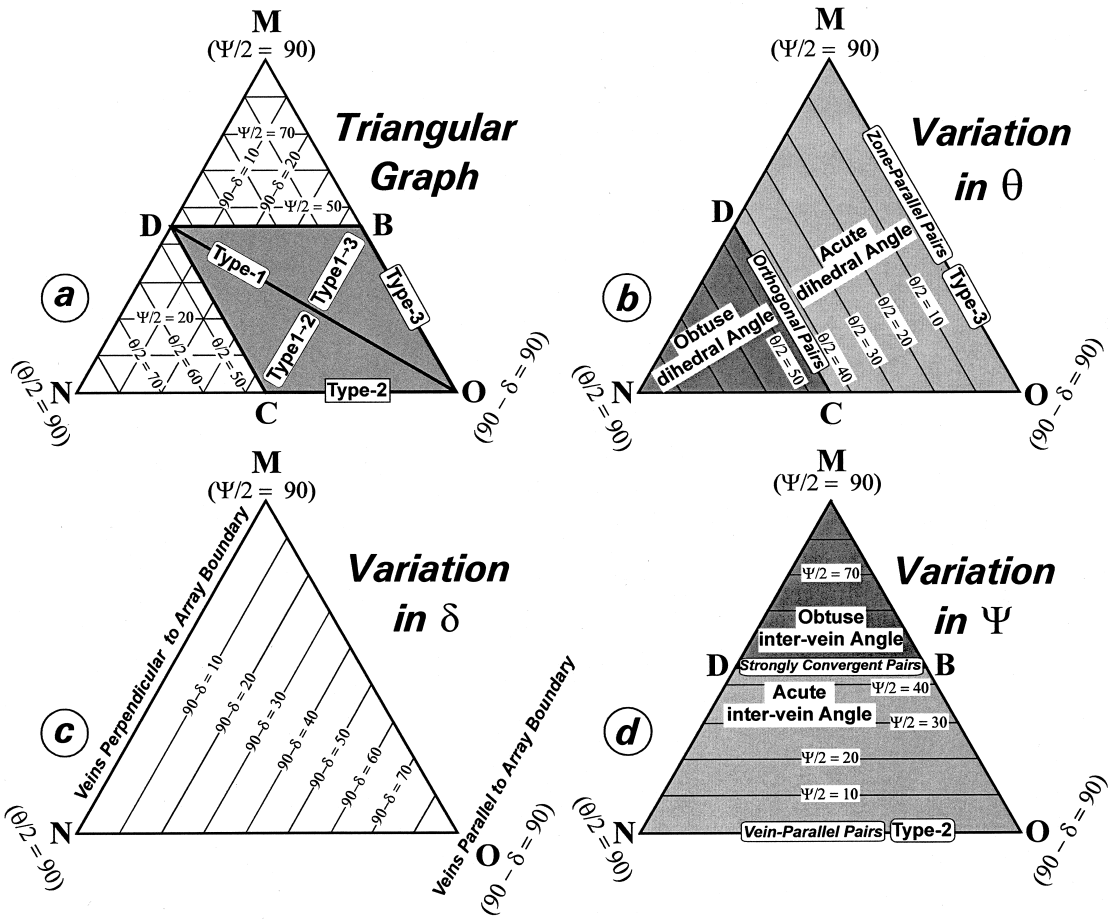

Fig. 2. (a) Triangular graph for plotting conjugate vein arrays of convergent configuration. Plots for all geometric variations of convergent vein arrays must fall within the rhombus-shaped field OBDC. (b) Variation in array dihedral angle θ. θ is equal to 0° and 90° for zone-parallel pairs and orthogonal pairs, which plot along the lines OM and CD, respectively. No example of conjugate array plots within the region (NCD) of obtuse θ. (c) Variation in vein-zone angle δ. δ is equal to 0° at point O and 90° along the line MN. (d) Variation in inter-vein angle ψ. ψ is equal to 0° and 90° for vein-parallel pairs (type-2) and strongly convergent pairs which plot along the lines ON and BD, respectively. No example of conjugate array plots within the region (MBD) of obtuse ψ.

boundary between convergent and divergent configurations.

5. Examples

Two aspects of natural examples of conjugate vein arrays need to be addressed for their representation in the triangular plot. First, different veins in a given array may not be inclined to the array boundary at the same angle. The representative vein-array angle δ in such cases is considered as the average of the angles that different veins make to the array boundary (Appendix A). Second, the vein-array angles in two complementary arrays of a conjugate pair may not be the same. The δ angle used for plotting such types of conjugate vein arrays is taken as the arithmetic mean of the representative vein-array angles in the two complementary arrays (Appendix A).

5.1. Chittaurgarh area (north-western India)

Conjugate vein arrays occur abundantly in the Middle Proterozoic to Early Cambrian sedimentary sequence in the vicinity of the Great Boundary Fault, near Chittaurgarh in northwestern part of India (Fig. 3a). The sedimentary sequence is folded into a series of open to gentle and N–S-trending, upright, non-plunging anticlines and synclines (Prasad, 1984). The best exposures of conjugate vein arrays occur in the sandstone beds occupying the core of the Fort syncline (Fig. 3a). That these vein arrays post-date the event of large-scale folding is evident by the fact that the vein arrays cut both the limbs and hinge zone of the Fort syncline without any marked variation in the orientation and/or geometry. Without exception, veins hosted in sandstone beds and limestone beds are composed of quartz and carbonate minerals, respectively. Such a strong lithological control on the composition

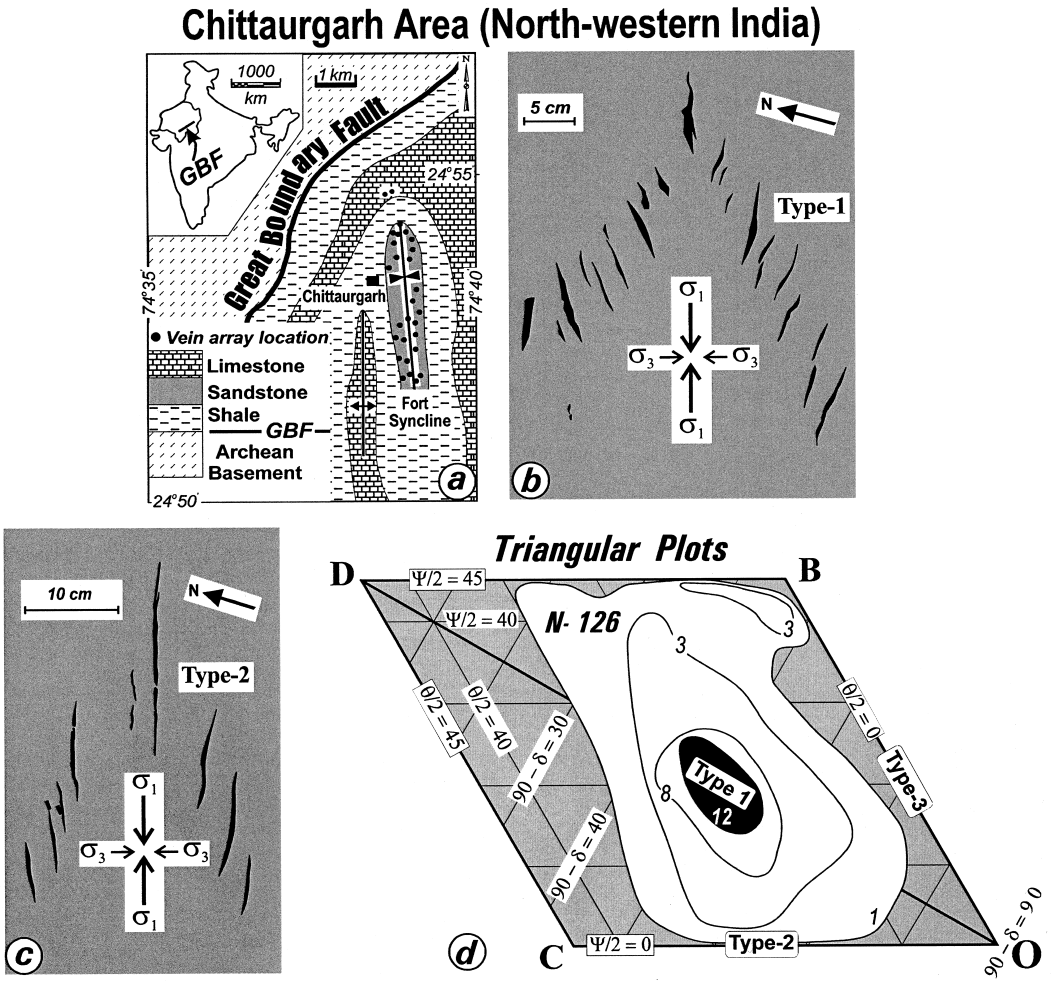

Fig. 3. Conjugate vein arrays in the Chittaurgarh area. (a) Geological map showing locations of the vein arrays (simplified after Prasad, 1984). Inset shows Great Boundary Fault (GBF) in India. (b) and (c) Representative geometries of different types of conjugate arrays occurring side by side on the same outcrop (traced from photographs of profile sections). (d) Triangular plots. Only the relevant rhombus-shaped region OBDC of the triangular graph (MNO in Fig. 2a) is shown. Contours—% per 1% area of the triangle MNO.

of the vein infillings implies a local or intraformational source for the mineralising fluids.

Of the different geometric types of conjugate vein arrays that are common in the Chittaurgarh area (Fig. 3b and c), type-1 pairs are predominant (Fig. 3d). A few conjugate pairs that are characterised by very low array dihedral angles, however, tend to approach type-3 geometry (Fig. 3d). Several lines of evidence imply that these geometrically different types of conjugate vein arrays were developed within a common stress system. For example: (i) the overprinting relationship amongst different types of conjugate vein arrays is characteristically inconsistent, (ii) despite considerable variation in the array dihedral angle from one conjugate pair to another, the bisectors of array dihedral angles in different pairs are parallel, and (iii) array boundaries and veins in different types of conjugate pairs have consistent sub-vertical to vertical dip and they are all of comparable size (cm–m).

Stress analyses on the different types of conjugate vein arrays yield consistent orientations of principal stresses. The bisectors of array dihedral angles in type-1 and type-2 pairs as well as the bisectors of inter-vein angle in type-1 pairs imply ENE–WSW and NNW–SSE orientations for maximum (σ_1) and minimum (σ_3) principal stresses, respectively (Fig. 4a–c). Furthermore, the veins that occur in type-2 pairs or within the intersection zone of type-1 pairs are, invariably, aligned perpendicular to the orientation of σ_3-axis (Fig. 4d and e).

Despite the fact that many conjugate vein arrays at Chittaurgarh are exposed only on flat bedding surfaces, some of the outcrops do allow three-dimensional measurement on type-1 pairs. The lower hemisphere

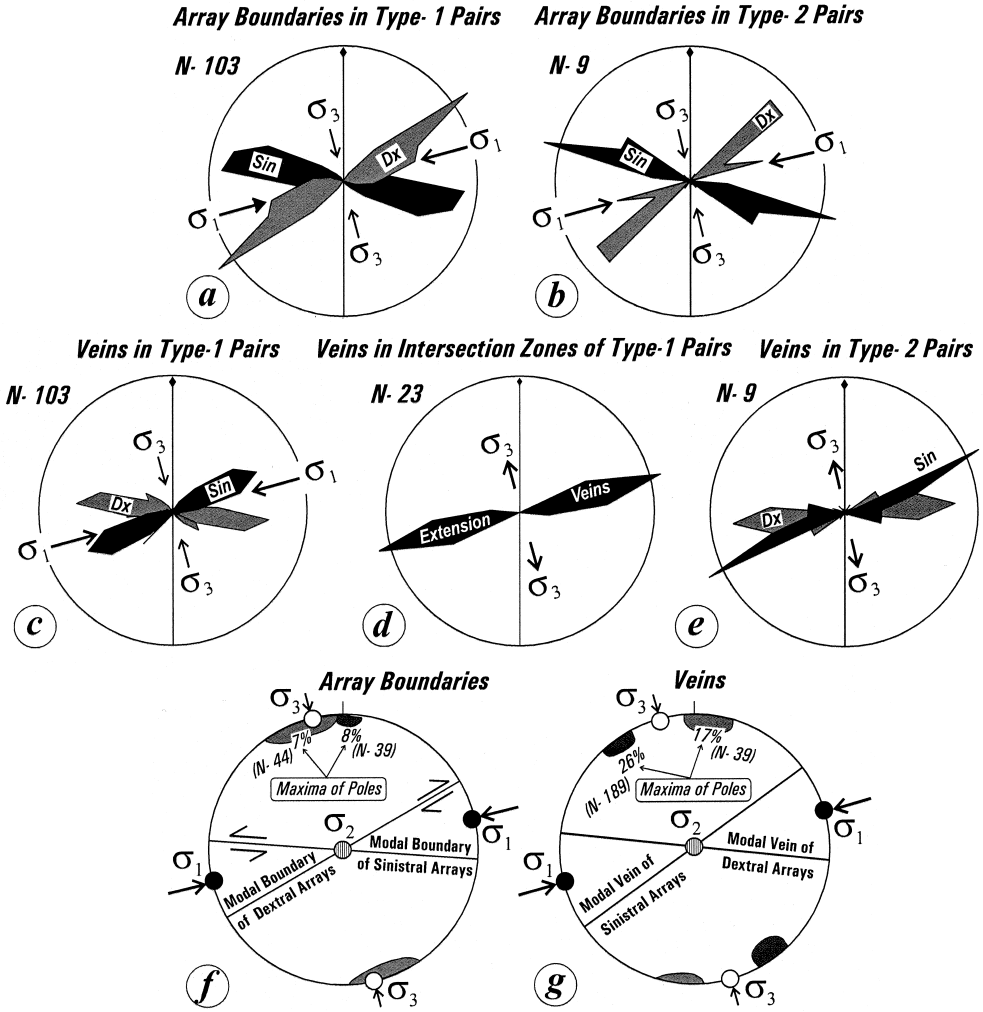

Fig. 4. Orientations of principal stresses inferred from conjugate arrays at Chittaurgarh. (a)–(e) Rose diagrams. Dx—Dextral array, Sin—Sinistral array. Diameter of circle—40% of the total data (N) in all the rose diagrams. (f) and (g) Stereoplots for array boundaries and veins in type-1 pairs. Contoured maxima of the poles and corresponding modal orientations of array boundaries and veins are shown in (f) and (g), respectively. Contour maxima—% per 1% of the area.

projections of the array boundaries and veins in such pairs indicate that these structures were developed in a strike-slip type of stress configuration defined by an ENE–WSW horizontal σ_1-axis, vertical σ_2-axis and NNW–SSE horizontal σ_3-axis (Fig. 4f and g). The orientations of σ_1- and σ_3-axes revealed by the rose diagrams and the stereoplots match well with each other (cf. Fig. 4a–e and f–g). Consistency in the orientations of principal stresses revealed by the independent analyses on type-1 and type-2 conjugate vein arrays suggests their development in a common stress system.

5.2. Mumbles area (Eastern Gower Peninsula, Swansea, UK)

The Lower Carboniferous carbonate sequence at Mumbles is folded into an ESE–WNW-trending, upright and gentle (interlimb angle 110–136°) Langland–Mumbles anticline that plunges at 17° towards S76°E (Fig. 5a, after Geological Survey of Great Britain, 1971; Srivastava et al., 1995). Numerous conjugate vein arrays characterised by steeply dipping to sub-vertical array boundaries and veins cut through both the limbs of the Langland–Mumbles anticline (Fig. 5c–f).

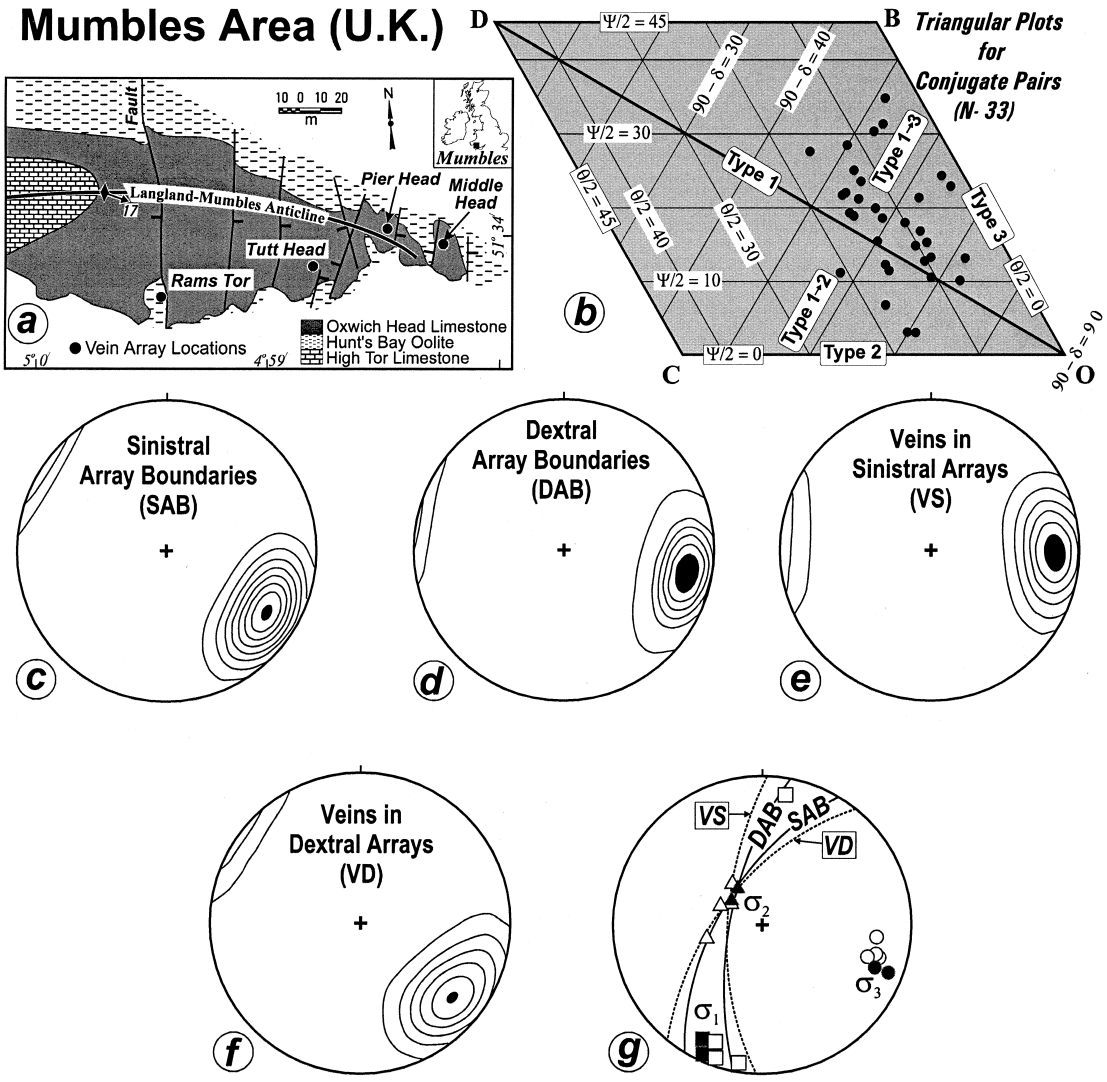

Fig. 5. Conjugate vein arrays in the Mumbles area. (a) Geological map showing locations of the vein arrays (after Geological Survey of Great Britain, 1971; Srivastava et al., 1995). (b) Triangular plots. (c)–(f) Contoured poles (Kamb contours every 5σ, $\sigma = 1.4$ and $N = 86$ in all the stereoplots). (g) Principal stress orientations. Symbols in black—Stresses revealed by Anderson's method on the conjugate sets of array boundaries and veins. Symbols in white—Stresses yielded by fault-slip methods (after Srivastava et al., 1995). SAB and DAB—Modal orientations of sinistral and dextral array boundaries, respectively. VS and VD—Modal orientations of veins in sinistral and dextral arrays, respectively.

Triangular plots of these conjugate vein arrays show that type-1 and transitional types (type-1 → 3) of geometries are predominant in this area (Fig. 5b).

Application of Anderson's method (Anderson, 1951) to the conjugate vein arrays at Mumbles implies their development in a stress configuration that is defined by a NNE–SSW horizontal maximum principal stress (σ_1), sub-vertical to vertical intermediate principal stress (σ_2) and ESE–WNW horizontal minimum principal stress (σ_3) (Fig. 5g). These results are consistent with those yielded by the application of the fault-slip methods on the vein arrays in the Mumbles area (Srivastava et al., 1995). The orientations of principal stresses imply that conjugate vein arrays at Mumbles were developed in a strike-slip type of stress configuration (Fig. 5g).

5.3. Other examples

Three angular parameters, θ, δ and ψ are measured on several published examples of conjugate vein arrays (Appendix A). The use of these examples is based on an assumption that the published illustrations exhibit profile views (Smith, 1995). Triangular plots of these examples show that conjugate vein arrays, conforming to geometry of the end-members (type-1 and type-2) and

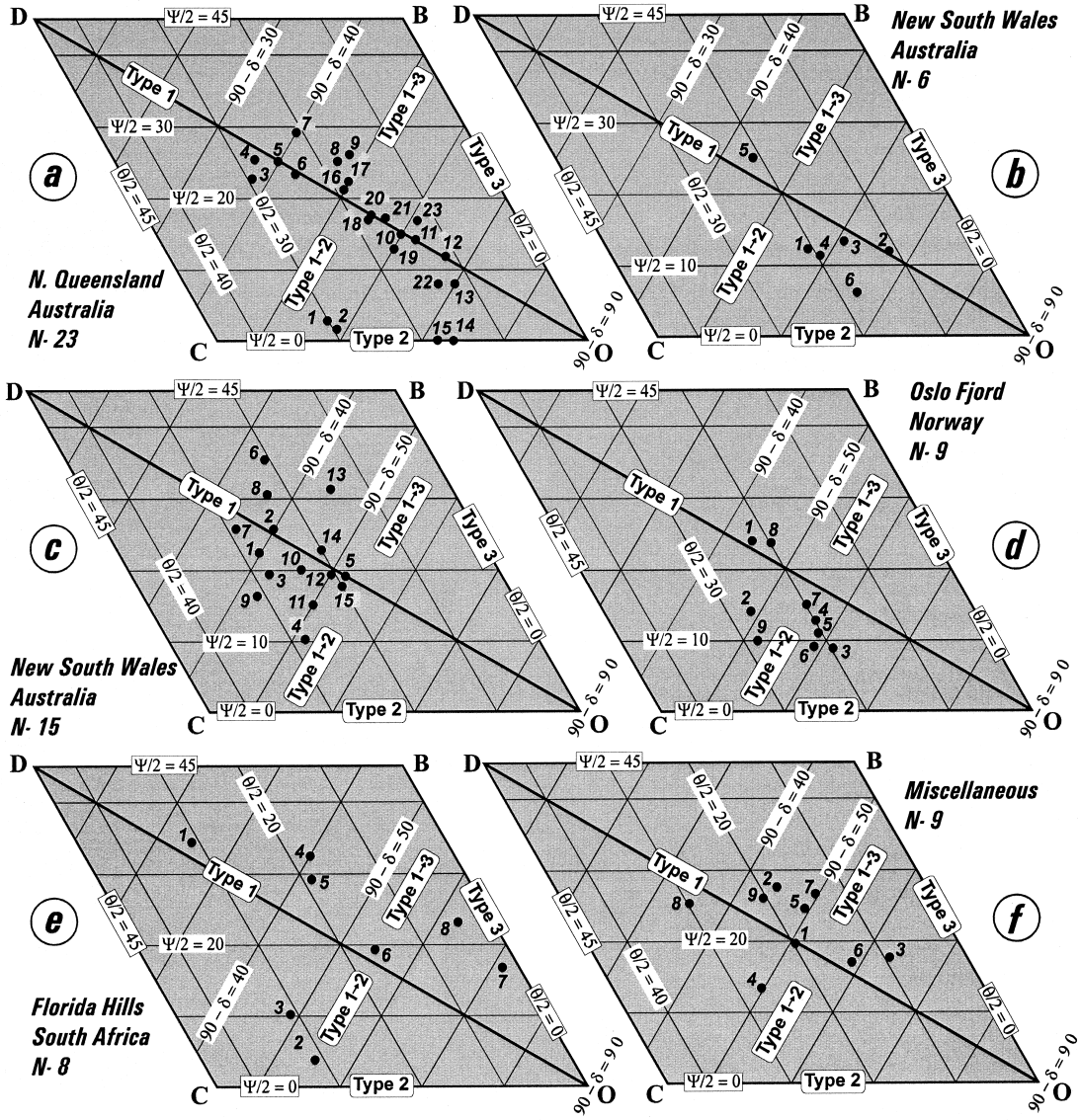

Fig. 6. Examples of triangular plots of conjugate arrays from published sources. (a) Calcite veins in Jack Formation limestone. (b) Quartz veins in Neranleigh Formation sandstone. (c) Quartz veins in Merrimbula Group sandstone. (d) Quartz veins in Silurian greywacke. (e) Quartz veins in Hospital Hill Series quartzite. (f) Miscellaneous plots (details and references are given in Appendix A). Plots—1, 2, 5 and 8—Quartz veins in sandstone; 3 and 7—Calcite veins in limestone; 4 and 6—Quartz veins in greywacke; 9—from clay model experiments.

transitional varieties (type 1 → 2 and type 1 → 3) of the spectrum, are common in natural rocks (Fig. 6a–f). Whereas type-1 pairs are most abundant, neither type-3 pairs nor divergent configurations of conjugate vein arrays are found to occur in any of the field examples (Table 1).

6. Discussion

Smith (1996) proposed a geometric continuum for conjugate vein arrays on the basis of relationship between two angular parameters: namely, θ and δ. Mutual relationships amongst three angular parameters, θ, δ and ψ, used in this article further strengthen the case for a continuous geometric spectrum of conjugate vein arrays.

Triangular plots for several examples show that different types of conjugate vein arrays occur commonly within a given area (Fig. 6). Case studies from Chittaurgarh and Mumbles support the inference that geometrically diverse types of conjugate vein arrays can develop in a common stress system. The common occurrence of meso-faults along the array boundaries and veins in the type-1 pairs at Chittaurgarh, implies that these array b??oundaries and veins are essentially shear structures. Poles to the veins that occur in type-2 pairs or within the intersection zones of type-1 pairs parallel the orientation of minimum principal stress (σ_3) inferred from independent analyses. Such a relationship implies that these veins are essentially extensional structures (Fig. 4d–e).

7. Conclusions

Type-1, type-2 and type-3 geometries define the extremities of a continuous geometric spectrum for conjugate vein arrays. All members of this geometric spectrum are represented in natural examples, except type-3 conjugate arrays that cannot form in rocks due to mechanical constraints. Similarly, divergent configurations of conjugate vein arrays also do not appear to occur in nature. Triangular plots are one convenient method for representation of conjugate vein arrays. Natural examples, when plotted on triangular plots, distinctly reveal that different geometrical types of conjugate arrays occur commonly within a given area.

Acknowledgements

I thank Prof. S.S. Srivastava and students for the help during the fieldwork in Chittaurgarh area during 1997–98. Constructive reviews by Dr. M.J. Rickard (New South Wales, Australia), Dr. Richard J. Lisle (Cardiff, UK) and an anonymous referee helped improve the manuscript considerably. This work was supported by Deep Continental Studies Program of the Department of Science and Technology, Government of India, and the UGC Research Award to the author.

Appendix A

Published examples of the conjugate vein arrays plotted in Fig. 6. *N*—Number of measurements, SD—Standard Deviation. δ, ψ and θ—as defined in Fig. 1(a). NA—Not available.

Fig. No.	Plot No.	Published source	δ in dextral array			δ in sinistral array			$90-\delta$ for pair	$\psi/2$ for pair	$\theta/2$ for pair
			N	SD	Mean	*N*	SD	Mean			
6a	1	Smith, 1997; fig. 1, Pair 1	NA	NA	NA	NA	NA	NA	57.0	3.0	30.0
6a	2	Smith, 1997; fig. 1, Pair 2	NA	NA	NA	NA	NA	NA	59.0	1.5	29.5
6a	3	Smith, 1997; fig. 1, Pair 3	NA	NA	NA	NA	NA	NA	38.0	22.5	29.5
6a	4	Smith, 1997; fig. 1, Pair 4	NA	NA	NA	NA	NA	NA	37.0	25.0	28.0
6a	5	Smith, 1997; fig. 1, Pair 5	NA	NA	NA	NA	NA	NA	40.0	25.0	25.0
6a	6	Smith, 1997; fig. 1, Pair 6	NA	NA	NA	NA	NA	NA	43.0	23.0	24.0
6a	7	Smith, 1997; fig. 1, Pair 7	NA	NA	NA	NA	NA	NA	40.0	29.0	21.0
6a	8	Smith, 1997, fig. 1, Pair 8	NA	NA	NA	NA	NA	NA	47.0	25.0	18.0
6a	9	Smith, 1997, fig. 1, Pair 9	NA	NA	NA	NA	NA	NA	48.0	26.0	16.0
6a	10	Smith, 1997, fig. 1, Pair 10	NA	NA	NA	NA	NA	NA	60.0	15.0	15.0
6a	11	Smith, 1997, fig. 1, Pair 11	NA	NA	NA	NA	NA	NA	62.0	14.5	13.5
6a	12	Smith, 1997, fig. 1, Pair 12	NA	NA	NA	NA	NA	NA	67.0	12.0	11.0
6a	13	Smith, 1997, fig. 1, Pair 13	NA	NA	NA	NA	NA	NA	70.0	8.0	12.0
6a	14	Smith, 1997, fig. 1, Pair 14	NA	NA	NA	NA	NA	NA	74.0	0.0	16.0

6a	15	Smith, 1997, fig. 1, Pair 15	NA	NA	NA	NA	NA	NA	72.0	0.0	18.0
6a	16	Smith, 1997, fig. 1, Pair 16	NA	NA	NA	NA	NA	NA	50.0	21.0	19.0
6a	17	Smith, 1997, fig. 1, Pair 17	NA	NA	NA	NA	NA	NA	50.0	22.0	18.0
6a	18	Smith, 1997, fig. 1, Pair 18	NA	NA	NA	NA	NA	NA	55.0	17.0	18.0
6a	19	Smith, 1997, fig. 1, Pair 19	NA	NA	NA	NA	NA	NA	60.0	13.0	17.0
6a	20	Smith, 1997, fig. 1, Pair 20	NA	NA	NA	NA	NA	NA	55.0	17.5	17.5
6a	21	Smith, 1997, fig. 1, Pair 21	NA	NA	NA	NA	NA	NA	57.0	17.0	16.0
6a	22	Smith, 1997, fig. 1, Pair 22	NA	NA	NA	NA	NA	NA	68.0	8.0	14.0
6a	23	Smith, 1997, fig. 1, Pair 23	NA	NA	NA	NA	NA	NA	61.0	17.0	12.0
6b	1	Smith, 1996, fig. 2, Pair 1	NA	NA	NA	NA	NA	NA	57.0	12.5	20.5
6b	2	Smith, 1996, fig. 2, Pair 2	NA	NA	NA	NA	NA	NA	67.0	12.0	11.0
6b	3	Smith, 1996, fig. 2, Pair 3	NA	NA	NA	NA	NA	NA	61.0	13.5	15.5
6b	4	Smith, 1996, fig. 2, Pair 4	NA	NA	NA	NA	NA	NA	59.0	11.5	19.5
6b	5	Smith, 1996, fig. 2, Pair 5	NA	NA	NA	NA	NA	NA	44.0	25.0	21.0
6b	6	Smith, 1996, fig. 2, Pair 6	NA	NA	NA	NA	NA	NA	66.0	6.5	17.5
6c	1	Rixon et al., 1983; fig 12a, Pair 1	4	53.00	3.36	8	47.00	2.94	40.0	22.0	28.0
6c	2	Rixon et al., 1983; fig 12a, Pair 2	6	53.33	3.93	8	47.00	2.94	40.0	25.5	24.5
6c	3	Rixon et al., 1983; fig 12a, Pair 3	7	47.35	7.32	8	47.00	2.94	43.0	19.0	28.0
6c	4	Rixon et al. 1983; fig 12a, Pair 4	7	47.35	7.32	4	28.50	3.93	52.0	10.0	28.0
6c	5	Rixon et al., 1983; fig 12b	9	36.00	8.07	8	39.68	4.33	52.0	19.0	19.0
6c	6	Rixon et al., 1983; fig 12c, Pair 1	6	58.80	9.92	8	53.56	2.66	34.0	35.0	21.0
6c	7	Rixon et al., 1983; fig 12c, Pair 2	6	58.80	9.92	5	50.20	1.92	35.5	25.5	29.0
6c	8	Rixon et al., 1983; fig 12d	7	50.71	10.85	10	55.70	5.14	37.0	30.0	23.0
6c	9	Rixon et al., 1983; fig 12e	4	45.75	3.86	5	48.4	12.17	43.0	16.0	31.0
6c	10	Rickard and Rixon, 1983; fig 1, Pair 1	12	48.33	4.33	6	39.50	1.64	46.0	20.0	24.0
6c	11	Rickard and Rixon, 1983, fig 1, Pair 2	12	48.33	4.33	9	31.55	3.84	50.0	15.0	25.0
6c	12	Rickard and Rixon, 1983; fig 1, Pair 3	4	48.25	1.50	9	31.55	3.84	50.0	19.0	21.0
6c	13	Rickard and Rixon, 1983; fig 1, Pair 4	4	48.25	1.50	6	43.66	5.46	44.0	31.0	15.0
6c	14	Rickard and Rixon, 1983; fig 1, Pair 5	15	41.66	3.37	6	43.66	5.46	47.0	23.0	20.0
6c	15	Rickard and Rixon, 1983; fig 1, Pair 6	15	41.66	3.37	4	35.00	0.00	52.0	18.0	20.0
6d	1	Weiss, 1972; fig 166B, Pair 1	7	49.14	3.43	3	43.50	2.64	44.0	24.0	22.0
6d	2	Weiss, 1972; fig 166B, Pair 2	9	39.44	6.16	3	43.50	2.64	48.5	14.0	27.5
6d	3	Weiss, 1972; fig 166B, Pair 3	4	25.50	5.25	4	33.25	2.75	61.0	9.0	20.0
6d	4	Weiss, 1972; fig 166B, Pair 4	3	32.66	3.00	4	33.25	2.75	57.0	13.0	20.0
6d	5	Weiss 1972, fig 166B, Pair 5	4	25.50	5.25	5	37.50	5.44	58.5	11.0	20.5
6d	6	Weiss, 1972; fig 166B, Pair 6	4	25.50	5.25	6	38.00	2.28	58.0	9.0	23.0
6d	7	Weiss, 1972; fig 166B, Pair 7	5	32.20	4.02	6	38.00	2.28	55.0	15.0	20.0
6d	8	Weiss, 1972; fig 166B, Pair 8	7	49.14	3.43	6	38.66	2.42	46.0	23.0	21.0
6d	9	Weiss, 1972; fig 166B, Pair 9	9	39.44	6.16	6	38.00	2.28	51.0	10.0	29.0
6e	1	Roering, 1968; fig 3, Pair 1	15	74.20	7.00	4	57.25	5.9	24.0	35.0	31.0
6e	2	Roering, 1968; fig 3, Pair 2	4	27.00	3.55	14	43.2	7.36	55.0	4.0	31.0
6e	3	Roering, 1968; fig 3, Pair 3	4	38.75	2.87	14	43.2	7.36	49.0	10.0	31.0
6e	4	Roering, 1968; fig 4, Pair 1	15	56.80	7.03	7	42.42	6.07	40.0	32.0	18.0
6e	5	Roering, 1968; fig 4, Pair 2	4	53.00	9.45	7	42.42	6.07	42.0	29.0	19.0
6e	6	Roering, 1968; fig 4, Pair 3	2	41.50	0.07	5	30.20	4.76	54.0	16.0	20.0
6e	7	Roering, 1968; fig 5	6	15.83	6.17	4	22.25	5.73	71.0	17.0	2.0
6e	8	Roering, 1968; fig 6B	2	35.00	0.00	3	18.33	1.50	63.0	23.0	4.0
6f	1	Price and Cosgrove, 1990; fig 18.22	6	40.58	3.16	8	37.68	5.33	51.0	20.0	19.0
6f	2	Sibson, 1996; fig. 7c	20	45.55	10.25	11	44.18	5.11	45.0	27.0	18.0
6f	3	Dietrich, 1989; fig. 10	11	26.77	3.42	9	26.88	1.38	63.0	17.0	10.0
6f	4	Ramsay and Graham, 1970; fig. 11	14	42.07	5.32	16	37.93	7.68	50.0	13.5	26.5
6f	5	Collins and De Paor, 1986; fig 3	10	46.50	2.59	7	34.28	3.80	50.0	24.0	16.0
6f	6	Weiss, 1972; fig. 166A	18	41.88	4.56	5	19.8	1.09	59.0	17.0	14.0
6f	7	Beach, 1975; fig. 2	15	40.53	4.45	10	40.40	2.71	50.0	26.0	14.0
6f	8	Beach, 1975; fig. 13	?5	59.80	1.79	6	50.16	4.60	35.0	25.0	30.0
6f	9	Smith, 1996; fig. 7	26	46.88	9.16	28	44.75	4.15	44.2	25.3	20.5

References

Anderson, E.M., 1951. The Dynamics of Faulting and Dyke Formation with Application to Britain, 2nd edn. Oliver and Boyd, Edinburgh.

Beach, A., 1975. The geometry of en-échelon vein arrays. Tectonophysics 28, 245–263.

Collins, D.A., De Paor, D.G., 1986. A determination of bulk rotational deformation resulting from displacements in discrete shear zones in the Hercynian Fold Belt of South Ireland. Journal of Structural Geology 8, 101–109.

Dietrich, D., 1989. Fold-axis parallel extension in an arcuate fold- and thrust belt: the case of the Helvetic nappes. Tectonophysics 170, 183–212.

Geological Survey of Great Britain, 1971. Ordnance survey sheet SS-68-NW on 1:10,560 or 6 inches to 1 mile scale.

Kelly, P.G., Sanderson, D.J., Peacock, D.C.P., 1998. Linkage and evolution of conjugate strike-slip fault zones in limestones of Somerset and Northumbria. Journal of Structural Geology 20, 1477–1493.

Prasad, B., 1984. Geology, sedimentation and paleogeography of the Vindhyan Supergroup, south-eastern Rajasthan. Memoirs of the Geological Survey of India 116, 107p.

Price, N.J., Cosgrove, J.W., 1990. Analysis of Geological Structures. Cambridge University Press, Cambridge.

Ramsay, J.G., Graham, R.H., 1970. Strain variation in shear belts. Canadian Journal of Earth Sciences 7, 786–813.

Rickard, M.J., Rixon, L.K., 1983. Stress configuration in conjugate quartz-vein arrays. Journal of Structural Geology 5, 573–578.

Rixon, L.K., Bucknell, W.R., Rickard, M.J., 1983. Mega kink folds and related structures in the Upper Devonian Merrimbula Group, south coast of New South Wales. Journal of the Geological Society of Australia 30, 277–293.

Roering, C., 1968. The geometrical significance of natural en-échelon crack arrays. Tectonophysics 5, 107–123.

Rothery, E., 1988. En-échelon vein array development in extension and shear. Journal of Structural Geology 10, 63–71.

Sibson, R.H., 1996. Structural permeability of fluid-driven fault-fracture meshes. Journal of Structural Geology 18, 1031–1042.

Smith, J.V., 1995. True and apparent geometric variability of en-échelon vein arrays. Journal of Structural Geology 17, 1621–1626.

Smith, J.V., 1996. Geometry and kinematics of convergent conjugate vein array systems. Journal of Structural Geology 18, 1291–1300.

Smith, J.V., 1997. Initiation of convergent extension fracture vein arrays by displacement of discontinuous fault segments. Journal of Structural Geology 19, 1369–1373.

Srivastava, D.C., Lisle, R.J., Vandycke, S., 1995. Shear zones as new type of paleostress indicator. Journal of Structural Geology 17, 663–676.

Weiss, L.E., 1972. The Minor Structures of Deformed Rocks—A Photographic Atlas. Springer-Verlag, Berlin.